Ostwald Ripening of β-Carotene Nanoparticles

Ying Liu, Kendra Kathan, Walid Saad, and Robert K. Prud'homme
Department of Chemical Engineering, Princeton University, Princeton, New Jersey 08544, USA
(Received 18 January 2006; published 17 January 2007)

Ostwald ripening, the interfacial-energy-driven dissolution and reprecipitation of solutes, becomes an increasingly significant problem for nanoparticle formulations. We present the first quantitative study of Ostwald ripening for nanoparticle dispersions. The Lifshitz-Slyozov-Wagner (LSW) theory of particle growth driven by diffusion is applied to study β-carotene nanoparticles with sizes of $O(100$ nm) formed by our block-copolymer protected Flash Nanoprecipitation process. A numerical implementation of the LSW theory that accounts for the original particle size distribution is presented. The predicted particle sizes from the numerical simulation are compared with the experimental results measured by dynamical light scattering. The results show quantitative agreement with no adjustable parameters. The addition of antisolvent results in the reduction of the ripening rate by dramatically decreasing bulk solubility.

DOI: 10.1103/PhysRevLett.98.036102 PACS numbers: 81.07.−b

Introduction.—Nanoparticles are currently widely studied, especially for the design and development of new pharmaceutical products from highly insoluble drugs [1–4]. The stability of nanoparticle dispersions can be affected by (1) agglomeration due to their high surface energy, (2) secondary crystallization, and (3) Ostwald ripening. Ostwald ripening is the process by which small particles shrink, due to enhanced solubility arising from their high curvature, and larger particles grow. The dependence of solubility, c, on the radius of a particle, R, is described by the modified version of the Kelvin equation [5],

$$c(R) = c_\infty \exp[2\gamma M/\rho \Re T R] = c_\infty \exp[\alpha/R], \quad (1)$$

where c_∞ is the bulk solubility of the dispersed phase, and α is the capillary length defined as,

$$\alpha \equiv \frac{2\gamma V_m}{\Re T}, \quad (2)$$

where γ is the interfacial energy, $V_m = M/\rho$ is the molar volume, M is the molecular weight of the solute with density ρ, $\Re$ is the gas constant, and T is the absolute temperature. The capillary length, α, defines the length scale below which curvature-induced solubility is significant. For particles with sizes over a few microns the differences in solubilities are negligible [$c(R) \cong c_\infty$], but for nanometer sized particles the effects can be substantial.

Ostwald ripening is a process that depends on both the physical chemistry of the compound and the particle size distribution. The theory of Ostwald ripening derives from the Lifshitz, Slyozov, and Wagner [6,7] (LSW) theory for the growth of particles during precipitation from supersaturated solution. Added to this is the effect of the particular initial distribution of particle sizes. The concept of Ostwald ripening has been *qualitatively* invoked to explain particle growth in a number of systems: predominantly metal and inorganic nanoparticles [8–10], emulsions systems [11–13], and the coarsening of phases in solid solutions [14,15]. It has not been demonstrated quantitatively for nanoparticle dispersions.

We have developed a novel nanoparticle formation process based on rapid micromixing to produce high supersaturations, which we term flash nanoprecipitation [16]. The particles are stabilized by the addition of a block copolymer to the solvent stream. The process depends upon the tuning of the kinetics of precipitation and the kinetics of block-copolymer assembly on the nanoparticle surface. Narrow particle size distributions are produced with exquisite control of particle size by controlling the supersaturation of the solute. Figure 1 shows the results of two experiments involving the precipitation of β-carotene nanoparticles and the stabilization with a poly(styrene)-*b*-poly(ethylene oxide) (PS-*b*-PEO) block copolymer. Particle distributions with mean diameters of 88 and 450 nm are shown. The stabilization of the nanoparticles by the block copolymer prevents particle aggregation, but the stabilizing polymer layer is open enough to allow

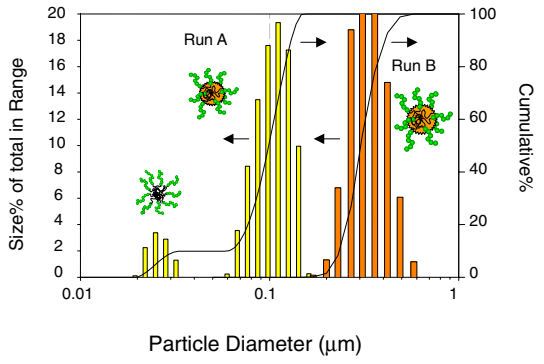

FIG. 1 (color online). Nanoprecipitation of β-carotene and PS (10 monomers)-*b*-PEO (68 monomers) as the static stabilizing block copolymer in THF using antisolvent water under two conditions. The final volume ratio of THF and water is 50:50 for both. Run A corresponds to a starting concentration of 0.52 wt% for both components fed at 2.8 m/s. Run B corresponds to 2.6 wt% for both components fed at 4.3 m/s.

solute mass transfer. In independent experiments we have studied the effective interfacial energy of the block copolymer layer and obtained a value of $\gamma = 1.9$ mJ/m^2 [17,18], which is typical of organic interfaces in water.

In this Letter we study the Ostwald ripening of β-carotene nanoparticles using dynamic light scattering to follow particle sizes. We first present the population balance model of Ostwald ripening following the development of Hoang, *et al.* [13], which they used to model the coarsening of emulsions. We describe the process of making the β-carotene nanoparticles in the next section. Finally, we compare the experimental results of aging and particle size growth to the simulations. All of the simulation parameters are determined by independent measurements. The model, without any adjustable parameters, accurately matches the experimental results on Ostwald ripening of β-carotene particles over a two-week period.

Ostwald ripening and LSW theory.—We adopt the formalism presented by Hoang *et al.* [13], who considered the Ostwald ripening of an emulsion. For nanoparticle growth by diffusion from a supersaturated solution in the quasi-steady-state limit, the Kelvin equation [Eq. (1)] can be linearized, since a $\alpha/R \ll 1$.

$$c(R) = c_\infty\left(1 + \frac{\alpha}{R}\right). \tag{3}$$

The diffusion flux of solute across the boundary of the particles is given by Fick's law,

$$j = D_m \frac{\partial c}{\partial r}\bigg|_{r=R}, \tag{4}$$

where D_m is the diffusion coefficient of the dispersed phase. The gradient is approximated as $\partial c/\partial r|_{r=R} = [\bar{c} - c(R)]/R$. From Eqs. (3) and (4) the growth rate of particle is,

$$\frac{dR}{dt} = \frac{D_m}{\rho R}\left(\Delta(t) - \frac{c_\infty \alpha}{R}\right), \tag{5}$$

where $\Delta(t) = \bar{c} - c_\infty$ is the supersaturation of the solution, which vanishes as $t \to \infty$. Thus for every value of the supersaturation, Δ, there exists a critical radius $R_c = c_\infty \alpha/\Delta$; for $R > Rc$ the particles grow, while for $R < R_c$ the particles dissolve. The particle size distribution function $f(R, t)$ obeys the continuity equation,

$$\frac{\partial f(R,t)}{\partial t} + \frac{\partial}{\partial R}\left[\frac{dR}{dt} f(R,t)\right] = 0. \tag{6}$$

The average size of particles is,

$$\bar{R} = \frac{\int_0^\infty dR f(R,t) R}{\int_0^\infty dR f(R,t)}. \tag{7}$$

The solution of the average radius growth rate was derived independently by Lifshitz, Slyozov, and Wagner [6,7],

$$\frac{d\bar{R}^3}{dt} = \frac{4}{9}\alpha D_m c_\infty. \tag{8}$$

The LSW theory is applied to Ostwald ripening of the nanoparticle dispersion by considering a distribution of particle sizes. The steps used for the numerical simulation of the Ostwald ripening process are: (1) as shown in Fig. 1, the particle size distributions obtained by flash nanoprecipitation can be represented by a lognormal distribution,

$$W(R) = \frac{1}{R\sqrt{2\pi\sigma}} \exp\left[-\frac{[\ln(R) - \langle \ln(R)\rangle]^2}{2\sigma^2}\right], \tag{9}$$

where $\langle \ln(R)\rangle$ is the number average of $\ln(R)$, and σ controls the breadth of the distribution. In the simulations, we arbitrarily use an initial number of particles equal to 20 000 ($i = 1, 2 \ldots$). Each particle has a specified number of molecules, which depends on the volume of the particle. (2) The number of molecules in a nanoparticle, n, varies with time as given by LSW theory:

$$\frac{dn}{dt} = 4\pi D_m c_\infty \alpha\left(\frac{R}{R_c} - 1\right), \tag{10}$$

where $n = \frac{4}{3}\pi R^3/V_m$. (3) From the mass balance of the disperse phase, the number average of the radius is the critical radius, which is updated for each time step j:

$$R_{c,j} = \sum_{i=1}^{N} R_{i,j}/N. \tag{11}$$

Particle size given by autocorrelation via dynamic light scattering (DLS).—The particle sizes are determined from the first cumulant fit of the DLS correlation function [19]. The first cumulant fit $\Gamma(q)$ is expressed as,

$$\frac{\Gamma(q)}{q^2} = \frac{\sum_{k=1}^{\max} n_k I_k D_k}{\sum_{k=1}^{\max} n_k I_k}, \tag{12}$$

where I_k is the scattering intensity of particle k, n_k is the number of particles of a given size, D_k is the diffusion coefficient of particle k, and the scattering wave vector is q. The first cumulant is related to the diffusion coefficient, D_0, by,

$$\frac{\Gamma(q)}{q^2} = D_0. \tag{13}$$

For dilute conditions, the Stokes-Einstein relation applies:

$$D_0 = \frac{kT}{6\pi\mu R}, \tag{14}$$

where μ is solvent viscosity. Combining Eqs. (12)–(14), we obtain an expression for the scattering intensity-weighted radius of the particles, $\bar{R}$:

$$\frac{6\pi\mu\bar{R}}{kT} = \frac{\sum_{k=1}^{\max,\infty} n_k I_k}{\sum_{k=1}^{\max,\infty} n_k I_k \frac{kT}{6\pi\mu R_k}}. \tag{15}$$

For the particles in the Rayleigh scattering range, the intensity of scattered light is proportional to the sixth power of the size for each particle [20,21]. This leads to the final expression for the diameter obtained by DLS

TABLE I. β-carotene physical-chemical properties and simulation parameters.

Property	Units	Value
β-carotene molecular weight	(g/mole)	536.9
Temperature	(K)	300
Molecular volume	(m^3/molecule)	8.91×10^{-28}
Crystal density	(kg/m^3)	1000
Interfacial energy	(mJ/m^2)	1.9

measurements:

$$\bar{R} \equiv R_{6-5} = \frac{\sum_{k=1}^{\max,\infty} n_k R_k^6}{\sum_{k=1}^{\max,\infty} n_k R_k^5}. \quad (16)$$

Therefore, the R_{6-5} moment of the size distribution is the appropriate moment to calculate from the simulations and to compare with the DLS experiments.

Experimental section.—β-carotene is a carotinoid that is enzymatically cleaved to produce two vitamin A molecules [22]. Its low solubility, nontoxicity, and commercial availability make it an attractive model compound to study particle stability. β-carotene nanoparticles were generated using a vortex mixer developed by Johnson and Prud'homme [17]. The block copolymer stabilizer comprised PS (10 monomers)-*b*-PEO (68 monomers). The vortex mixer geometry allows for high intensity mixing with different ratios of solvent to nonsolvent, which alters the supersaturation level during particle formation. THF with 1 wt% of PS-*b*-PEO and 1 wt% of β-carotene is mixed with water using the vortex mixer and two digitally controlled syringe pumps (Harvard Apparatus, PHD 2000 programmable, Holliston, MA). The β-carotene/polymer stream flow rate was varied between 6 and 60 ml/ min, and the water stream flow rate was fixed at 120 ml/ min. The sample was collected at the mixer outlet, and the particle sizes were determined by DLS (Brookhaven Instrument, BI-200SM, Holtsville, NY), consisting of double-pumped continuous NdYAG laser (Coherent Inc., wavelength 532 nm, 100 mW, Santa Clara, CA), and a photomultiplier with detection angle of 90°. The signal of the photomultiplier was analyzed by autocorrelation (ALV-Laser Vertriebsgesellschaft mbH, ALV-5000/E, Langen, Germany), yielding the time-averaged scattered average particle size and polydispersity index (PDI). The particle radius distribution is calculated also by ALV-5000/E, using the Stokes-Einstein equation from the decay time distribution function with the assumption that the scattering particles behave as hard spheres in dilute solution and within the Rayleigh-Debye theory.

The parameters used for β-carotene in the simulation are given in Tables I and II. The interfacial energy had been determined previously from measurements of block copolymer micellization [18,23].

The molecular diffusion coefficient, in Table II, is calculated according to the Stoke-Einstein equation,

$$D_m = 7.4 \times 10^{-8}\ \mathrm{T}\frac{(2.6 \times M_W)^{1/2}}{\mu V_m{}^{0.6}}. \quad (17)$$

β-carotene solubility in different solvents was experimentally measured using UV adsorption at 290 nm wavelength, and the mixed solvent viscosities were measured using an automated Ubbeholde capillary viscometer (Schott, Model CT460, and AVS 360, Mainz, Germany). The solubility of β-carotene decreases exponentially with antisolvent addition and can be fit by $c_\infty = 0.0126e^{24.9\phi}$, where c_∞ is the bulk solubility of β-carotene, and ϕ is the volume fraction of THF.

Results and discussion.—The experimental and numerical simulation results of the particle sizes versus time for β-carotene nanoparticles are shown in Fig. 2. The data shows the strong effect of solute solubility on Ostwald ripening. When the β-carotene solubility in the water:THF solution is 0.04 mM, the particles change size by less than 10 nm (13.7%) over 15 days. However, when the solubility is 1.67 mM they grow in size by 77 nm (62.7%). Changing the solvent (THF) to nonsolvent (water) ratio in the mixing process from 1:4 to 1:20 (volume:volume) reduces the solubility of β-carotene by a factor of about 40 and reduces the average particle growth rate by a factor of about 10. Therefore, an efficient way to significantly slow Ostwald ripening of the nanoparticles is to lower the solubility by antisolvent addition.

In the numerical simulations, σ and $\langle \ln R \rangle$ values were determined from the initial size distribution of the particles experimentally measured by DLS. The differences in initial particle sizes are due to the different supersaturations of β-carotene during particle formation; the values taken within 15 min of formation were used as the initial sizes. The numerical simulation prediction is given by the solid lines for each initial size and solubility condition. The growth rates are initially highest and decrease with time—the smaller particles disappear and the average particle radius increases. The decrease in growth rate is not due to a decrease in supersaturation over long periods

TABLE II. β-carotene solubility in mixed THF/water solutions.

Solvent THF to water ratio	Viscosity (Pa · s)	β-carotene solubility (mM)	β-carotene diffusion coefficient (m^2/s)
6:120	0.92×10^{-3}	0.04	2.07×10^{-9}
12:120	0.95×10^{-3}	0.12	2.00×10^{-9}
18:120	1.01×10^{-3}	0.35	1.90×10^{-9}
24:120	1.08×10^{-3}	0.85	1.77×10^{-9}
30:120	1.15×10^{-3}	1.67	1.66×10^{-9}

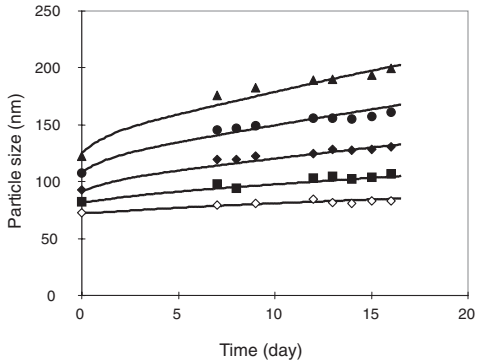

FIG. 2. Comparison of the time evolution of average particle sizes between numerical and experimental data for different tetrahydrofuran to water ratios [(ml/ min)/(ml/ min)]: ▲ 30:120, ● 24:120, ◆ 18:120, ■ 12:120 and ◇ 6:120. The particle size is twice $\bar{R} \equiv R_{6-5}$ shown in Eq. (16).

of time. As shown in the LSW theory the supersaturation in the initial mixing process is rather rapidly relieved as the particles are formed and the background solution saturation becomes, essentially, the equilibrium value. The growth due to Ostwald ripening is not a *continued* growth of all particles in response to supersaturation in the bulk solution, rather it is a redistribution of mass among particles based on their curvature. Therefore, Ostwald ripening is independent of particle concentration.

The importance of these results is that they demonstrate the ability to predict Ostwald ripening of nanoparticles from first principles. *A priori* projections of long term stability can be made. The model also enables sensitivity studies of the ripening to the details of the initial particle size distribution. This should aid in decisions as to particle formation processes that are most appropriate for nanoparticle formation. Finally, the demonstration also points the way to ''accelerated'' testing methodologies whereby the addition of cosolvents to a liquid phase can be used to test particle stability over relative short times and enable predictions of stability of the pure system over much longer time scales.

In the simulation, no interfacial barrier to dissolution or incorporation is considered. This appears to be the case for these β-carotene nanoparticles. It also brings up the possibility of altering particle stability by various surface coating techniques. That is, coatings could be employed to alter the mass transfer rate at the particle surface. The success of the model means that the effect of surface coatings can be evaluated because the coarsening kinetics in the absence of a barrier can be predicted. Finally, we note that the polymer stabilized nanoparticles we have formed prevent particle growth by agglomeration. The dilute steric stabilizing layer is less than 10 wt% PEO [24] and this has negligible effect on solute diffusion from or to the particle surface [25].

Conclusion.—The experimentally measured nanoparticle sizes as a function of time are reported and quantitatively fitted by numerical simulations based on the LSW theory and a population balance. The simulation incorporates both the physical-chemical properties of the solute comprising the particle phase, and also the initial particle size and distribution. The lower the solute solubility in the solvent phase, the slower the growth rate—as predicted by the LSW theory. A tenfold increase in particle growth rate accompanies a 40-fold increase in solubility. The narrower the initial size distribution, i.e., the smaller the difference between the higher-solubility small particles and the lower-solubility large particles, the more stable is the dispersion. This is the first demonstration of the ability to quantitatively predict the coarsening *via* Ostwald ripening of nanoparticle dispersions using independently measured physical properties and the LSW theory. It provides the framework for projecting stability of other formulations and for studying new methodologies of stabilizing nanoparticles by modifying surface incorporation kinetics.

[1] J. H. Hu *et al.*, Drug Development and Industrial Pharmacy **30**, 233 (2004).
[2] K. Kataoka *et al.*, Adv. Drug Delivery Rev. **47**, 113 (2001).
[3] E. Merisko-Liversidge *et al.*, Pharm. Res. **21**, 1545 (2004).
[4] B. E. Rabinow, Nat. Rev. Drug Discov. **3**, 785 (2004).
[5] D. J. W. Grant and H. G. Brittain, *Physical Characterization of Pharmaceutical Solids* (Marcel Dekker, New York, 1995).
[6] I. M. Lifshitz and V. V. Slyozov, J. Phys. Chem. Solids **19**, 35 (1961).
[7] C. Wagner, Z. Elektrochem. **65**, 581 (1961).
[8] K. Kimijima and T. Sugimoto, J. Phys. Chem. B **108**, 3735 (2004).
[9] J. P. Wilcoxon and P. Provencio, J. Phys. Chem. B **107**, 12 949 (2003).
[10] F. Huang *et al.*, Nano Lett. **3**, 373 (2003).
[11] A. S. Kabalnov and E. D. Shchukin, Adv. Colloid Interface Sci. **38**, 69 (1992).
[12] P. Taylor, Adv. Colloid Interface Sci. **75**, 107 (1998).
[13] T. K. N. Hoang *et al.*, Langmuir **20**, 8966 (2004).
[14] P. W. Voorhees, Annu. Rev. Mater. Sci. **22**, 197 (1992).
[15] C. Jacobs and R. H. Mulle, Pharm. Res. **19**, 189 (2002).
[16] B. K. Johnson and R. K. Prud'homme, Australian J. Chem. **56**, 1021 (2003).
[17] B. K. Johnson, Ph.D. thesis, Princeton University, 2003.
[18] B. K. Johnson and R. K. Prud'homme, Phys. Rev. Lett. **91**, 118302 (2003).
[19] W. B. Russel, *Colloidal Dispersions* (Cambridge University Press, Cambridge, England, 1989).
[20] G. F. Bohren and D. R. Huffman, *Absorption and Scattering of Light by Small Particles* (John Wiley & Sons, Inc., New York, 1983).
[21] B. J. Berne and R. Pecora, *Dynamic Light Scattering: With Applications to Chemistry, Biology and Physics* (John Wiley & Sons, Inc., New York, 1976).
[22] J. Glover, Vitamins and Hormones—Advances in Research and Applications **18**, 371 (1960).
[23] O. Sohnel *et al.*, Ind. Eng. Chem. Res. **27**, 1721 (1988).
[24] D. T. Auguste *et al.*, Biomaterials **27**, 2599 (2006).
[25] L. Haggerty *et al.*, Polymer **29**, 1058 (1988).